# Exploring the potential of chitosan/aragonite biocomposite derived from cuttlebone waste: Elaboration, physicochemical properties and in vitro bioactivity

Youssef Ait Hamdan, Samia Elouali, Hassane Oudadesse, Bertrand Lefeuvre, Mohammed Rhazi

# Exploring the potential of chitosan/aragonite biocomposite derived from cuttlebone waste: Elaboration, physicochemical properties and *in vitro* bioactivity

**Youssef Ait Hamdan[a,b*], Samia Elouali[a,c], Hassane Oudadesse[b], Bertrand Lefeuvre[b], Mohammed Rhazi[a*]**

[a]*Interdisciplinary Laboratory in Bio-Resources, Environment and Materials, Higher Normal School, Cadi Ayyad University, 4000, Marrakech, Morocco.*

[b]*Univ Rennes, CNRS, ISCR-UMR 6226, F-35000 Rennes, France.*

[c]*Laboratory of Polymeric and composite Materials, UMONS, Belgium.*

E-mail: youssef.aithamdan.ced@uca.ac.ma



## 1. Introduction

Chitin, poly (β-(1→4)-N-acetyl-D-glucosamine), is one of the most abundant functional polysaccharides on earth. Marine and terrestrial fauna are the main sources of this

polysaccharide [1]. Depending on its source, chitin occurs in a state where it is associated mainly with calcium carbonates [2]. Cuttlefish bone is an inexpensive and readily available biomaterial, it has a structure consisting of a hard-dorsal shield and a brittle ventral shell with a structure forming interconnected porous chambers [3, 4]. It is composed of calcium carbonate ($CaCO_3$) in its allotropic variety "aragonite" associated with a complex of β-chitin and proteins that represents a small amount (3 to 5%) of organic matter [3]. The organization of the chitinous spindles between the aragonitic mineral layers constitutes the structural framework of a cuttlebone and seems to ensure the mechanical stability and the buoyancy of a skeleton [5].

Industrially, the amount of chitinous coproducts based on cuttlebone discarded annually in some coastal areas of Morocco, is considerable and harmful, is about 1,732, 034 tons [6,7]. At this scale, the production of α-chitin is mainly from crab and shrimp shells. While the production of β-chitin is from squid shells. The interest in β-chitin is due to its specific physicochemical properties. It has a higher solubility than α-chitin [8, 9]. Moreover, it is characterized by a high reactivity during N-deacetylation, which depends on the low number of intermolecular hydrogen interactions. Also, it offers the possibility to elaborate chitosans that are strongly deacetylated [6].

Chitosan, poly (β-(1→4)-N-acetyl-D-glucosamine) is the derivative of chitin by deacetylation with a degree of over 50% [10]. As a result of this reaction, chitosan has free and functional amine groups that promote complete solubility in acidic organic solvents. Chitosan is used in many current and potential applications [11] such as food [12], medicine [13], water treatment, cosmetics [14, 15], textile, paper and biotechnology [16-17], due to its properties of solubility, biocompatibility and biodegradability [18] [19] [20] [21] [22] [23]. As cuttlefish bone is a biological composite material incorporating the arago-chitinous complex, like nacre (composed of 95% aragonite and 5% chitin), it has an excellent in vivo biocompatibility and biodegradability properties, and greater osteogenic potential than hydroxyapatite [24]. Research has been carried out on biocomposites combining commercial chitosan and synthetic calcium carbonate cement, with the aim of exploring their applications as bone substitutes [25].

To our knowledge, no research to date has exploited cuttlebone waste to develop biocomposites with physicochemical and biological properties suitable for biomedical applications. Inspired by the composition of this biological material, we have undertaken, for the first time, a study of the physico-chemical properties and in vitro bioactivity of chitosan (CHS) and aragonite (ArgS) derived from cuttlebone waste discharged by processing facilities along the Moroccan

Atlantic coast. Bioactivity was assessed by examining the formation of a hydroxyapatite layer in simulated human plasma. This layer shows similarities to that which forms naturally in human bone. Analytical and characterization methods and techniques including, Fourier transform infrared analysis (FTIR), X-ray diffraction (XRD) and Scanning Electron Microscopy (SEM), proton Nuclear Magnetic Resonance ($^1$H-NMR) were applied. The investigations were completed by quantitative elemental (ICP-OES) and thermal (TGA/DSC) analyses.

## 2. Materials and methods

### 2.1. Preparation of cuttlefish bone

The bones of *Sepia officinalis* were collected on the coast of the Marrakech-Safi region (Morocco), and washed several times with distilled water to remove organic debris and then dried at 80°C for 24 h. The cuttlefish bone has two faces, a dorsal and a ventral one (Fig.1), the ventral part will be used to isolate the aragonite, and the dorsal part will be used to extract the β-chitin.

### 2.2. Aragonite isolement

To isolate aragonite the ventral part was used. Pieces were cut and washed with bidistilled water, then heat-treated at 300°C for 3h, to remove all organic debris. After heat treatment, the pieces were ground to a fine powder (< 40 μm).

### 2.3. β-Chitin extraction and chitosan preparation

To extract β-chitin, we adopted the process developed by Ait Hamdan *et al*., [26]. Demineralization was performed at room temperature with 0.55 M HCl baths 1:20 (w/v) for 60 min. Then, deproteinization step consisted of using NaOH (0.3M) at 80-90°C for 1 h. This treatment was repeated until the bath became clear, indicating protein removal. To prepare chitosan, we adopted the process described by Broussignac [27]. This process consists in using a mixture of 50% potassium hydroxide, 25% ethanol (96°) and 25% mono-ethylene glycol, this reaction being almost anhydrous. Afterwards, 10 g of β-chitin was added progressively to 500 ml of mixture under stirring at 120°C for 10 hours. Then, the chitosan was filtered, washed with water to neutrality, then with ethanol/acetone (1/1, W %) and dried at 40°C.

### 2.4. Preparation of chitosan/aragonite biocomposite

The biocomposite, composed of aragonite and chitosan polymer, was developed using the freeze-drying method. Initially, powdered aragonite microparticles (< 40 μm) were dispersed in a solution of bidistilled water (3% w/v), then this mixture was added continuously to the chitosan solution (1% w/v) dissolved in acetic acid (0.3%, v/v) and stirred for 2 hours at 1200 rpm using magnetic stirring. Next, the mixture of Aragonite and chitosan polymer was frozen at -20°C for 24 hours, then immediately transferred to a freeze-dryer at -60°C for 24 hours to remove solvents. To neutralize the acetic acid radicals remaining in the composites, which could have an impact on the pH of the plasma during in vitro testing, the biocomposite obtained was immersed in a NaOH solution (5% w/v), followed by washing with deionized water. Finally, the aragonite/chitosan biocomposite underwent further freezing and freeze-drying for 24 hours to completely remove the solvent [28, 29-30].

### 2.5. In vitro bioactivity evaluation in simulated body fluid

The in vitro bioactivity of the biomaterials was assessed by immersion in simulated body fluid (SBF). To prepare this solution, NaCl, $NaHCO_3$, KCl, $K_2HPO_4.3H_2O$, $MgCl_2.6H_2O$ and $CaCl_2$ were dissolved in deionized water, and the pH was adjusted to 7.4 using $(CH_2OH)_3CNH_2$ and HCl (6N) [31-32]. The composition of the SBF solution is similar to that of human blood plasma, as shown in Table 1. Samples of ArgS powder and CHS/ArgS biocomposite were immersed in the SBF solution for durations of 0 (control), 3, 7, 15 and 30 days, at a body temperature of 37°C. At the end of immersion, samples were removed, rinsed with deionized water to stop exchange reactions, and then washed with absolute alcohol. Samples were dried and stored for further analyses of the formation of a hydroxyapatite (HA) layer on their surface, verified by FTIR and SEM. SBF solutions were stored under refrigeration for evaluation of ionic concentrations by ICP-OES (inductively coupled plasma optical emission spectrometry).

### 2.6. Physicochemical characterization

#### 2.6.1. NMR characterization

$^1$H-NMR was performed on a 400 MHz Brucker where the samples (20 mg) are solubilized in a solution of 0.9 ml DCl at 20% in $D_2O$ for chitin and a solution of 0.5 ml DCl at 2% in $D_2O$

for chitosan. These samples are then heated at 70°C for 1h and the NMR chemical shifts are reported in ppm.

### 2.6.2. Potentiometry titration

Chitosan was first solubilized in HCl (0.1M) solution, followed by titration with NaOH (0.1M) solution. The degree of deacetylation was then determined by equation [10, 33]:

$$\mathbf{NH_2 = 1\text{-}DA = \frac{16{,}1\ (X2-X1)}{m-m0} \times N}$$

Which ($x_2$-$x_1$) is the difference of two turning zones, m is the weight of chitosan, $m_0$ the water content in chitosan sample, N is the normality of NaOH solution, 16.1 is the weight of $NH_2$ group.

### 2.6.3. Molecular weight determination

Ubbelohde capillary viscometer (0.5-3 $mm^2/s$, 20 ml) was used to determine the viscosity and molar mass of chitosan at 25°C using the Mark Houwink equation [34]:

$$[\eta] = K.\ [M]^a$$

With [η] the intrinsic viscosity (ml/g); M the viscometric molar mass; K= 0.070 and a = 0.081. The solvent is a mixture of 0.3 M acetic acid and 0.2 M sodium acetate.

### 2.6.4. TGA and DSC measurments

Thermogravimetry (TGA) and differential scanning calorimetry (DSC) measurements were performed using a Setaram Labsys 1600TG-DTA/DSC under $N_2$ gas atmosphere at 0.1 MPa. Chitin and chitosan were heated from 40°C to 650°C, while aragonite was heated from 40°C to 950°C, at a heating rate of 5°C min for 4 h.

### 2.6.5. Scanning electron microscopy (SEM) analysis

The morphological structure of all samples was assessed using a Quanta 200 scanning electron microscope. Before the start of the morphological analysis, samples have been metalized using a layer of gold-palladium.

### 2.6.6. FT-IR characterization

FT-IR spectra were performed on Jasco 4600A Gemini FT-IR sampling spectrometer. Spectra were collected from 400 to 4000 $Cm^{-1}$ with 32 scans at 4 $Cm^{-1}$ resolution.

### 2.6.7. X-ray Diffraction (XRD) Analysis

X-ray diffraction measurements are made with Rigaku III diffractometer with Cu radiation (40 kV, 30 mA at 1, 54184 Å and acceptance slit at 0.1 mm), the results are obtained with scan angle from 5° to 60° (1° $min^{-1}$). Also, the crystallinity index ($I_{Cr}$) of chitin and chitosan was calculated by the equation [35-36]:

$$I_{Cr} = \frac{(Ic - Ia)}{Ic} \times 100$$

With $I_c$ and $I_a$ are the intensities of the crystalline (2θ ≈19°- 20°) and amorphous (2θ ≈ 8°-10°) regions, respectively.

### 2.6.8. ICP-OES Analysis

Inductively Coupled Plasma Optical Emission Spectroscopy (ICP-OES), iCAP 7000 (ThermoFisher Scientific), with a high sensitivity of less than 1 ppm, was used to study the ventral and dorsal faces of cuttlefish bone, and to assess ion exchange between SBF and biomaterials before and after immersion.

## 3. Results and discussion

### 3.1. Chitin, Chitosan and Aragonite production

One of the problems encountered in the extraction of pure chitin close to the native form is to minimize deacetylation and degradation of macromolecular chains during the extraction process. In our study, we adopted the chemical process described by Ait Hamdan et al., [26], it allows to obtain pure, highly acetylated chitin as close as possible to the native form. The results of the chemical composition analysis by ICP-OES of the dorsal and ventral side are presented in Table 2. On the ventral side, the Ca content is twice as high (141.8 ± 0.6 ppm) as on the dorsal side, proving that it consists exclusively of aragonite (62% of all cuttlefish bone) stabilized by other mineral elements (Na, Sr, P, Al, Si and Zn) at low levels (Table 2). On the

dorsal side, which was used for chitin extraction, we spent 4 acid baths (HCl; 0.55M), which explained by the significant mineral content in this part, estimated to be around 50%, including 30% of Ca from the total minerals[37]. The process of extraction of chitin and obtaining chitosan involves several steps (Fig.2). The extracted chitin is perfectly white and therefore does not require a bleaching step and is extracted with a yield of 11%, this yield is relatively close to some values reported in the literature [38].

### 3.2. Aragonite, Chitin and chitosan characterization

**FTIR analysis** of chitin and chitosan is shown in Figure 3 and Table 3. Both polymers show a strong band observed between 3260 and 3560 $cm^{-1}$, representing bond stretching of the $-NH_2$ and -OH groups [39]. In the spectrum of chitin, a band was observed at 2869-2938 $cm^{-1}$, attributed to the C-H vibration of $-CH_3$. In addition, this spectrum shows a peak observed at 1641.07 $cm^{-1}$ attributed to the stretching and vibration of the carbonyl group, C=O of acetamide ($-NHCOCH_3$) and a peak at 1555.70 $cm^{-1}$ indicating the flexural vibration of -NH [40]. The peak at 894, 66 $cm^{-1}$ is a ring stretching band characterizing the β-1,4 glycosidic bonds. The absorption peak at approximately 1081.87 $cm^{-1}$ is the stretching vibration of the -C-O-C bridge of the glucosamine ring. These results are therefore in agreement with those of [41, 42, 43] and show that it is indeed β-chitin. After the alkaline treatment of chitin, a remarkable change in the intensity of the bands corresponding to the -CO and -NH amide bonds in chitosan were observed, providing evidence that a deacetylation reaction is occurring. For FTIR of aragonite (Fig.3a), it shows characteristic bands attributed to the phosphate group observed at 1085 $cm^{-1}$, 714 $cm^{-1}$ attributed to the -C-O bond and 851 $cm^{-1}$ for the -OH group [44, 45]. Moreover, bands derived from $CO_3^{2-}$ ions vibrations are observed at 1480 $cm^{-1}$ and also bands close to 1790 $cm^{-1}$ and 2525 $cm^{-1}$ can also be attributed to carbonate ions vibrations [45].

XRD analysis of the dorsal surface of cuttlefish bone reveals the coexistence of two distinct components: aragonite, an inorganic component identifiable by several peaks of varying intensity, and chitin-protein, an organic component presenting two peaks of intensity at 8-20° (2θ), suggesting the presence of chitin bound to both protein and aragonite (Fig.4). This discovery underlines the need for a specific chemical treatment process to extract chitin in a pure and exploitable way. After the demineralization and deproteinization steps, two large intense crystalline reflections observed at 8.17° and 19.50° (2θ) corresponding to the (020) and (110) planes (Fig.5). These reflections are attributed to β-chitin, which is the organic constituent of the cuttlebone skeleton, confirming that pure chitin was obtained [44]. After deacetylation

of chitin, two peaks are observed at 10° (2θ) and 20° (2θ), which are characteristic of chitosan (Fig.5) [46], with a decrease in the intensity of the amorphous peak compared to chitin, which explains the decrease in its crystallinity confirmed by the calculation of the crystallinity index (ratio of amorphous regions to crystalline regions) (Table 4). One could say that deacetylation seems to exert an effect on crystallinity. In the ventral part, XRD phase analysis shows that the only mineral phase present in the bone is aragonite with the three most intense reflections involve the (012), (111), and (221) planes corresponding to 26,26° (2θ), 33,33° (2θ), and 45,90° (2θ) respectively (Fig.6). All observed intensities agree well with the reference model for aragonite when compared with that of calcite (Fig.7) [47]. It shows that cuttlefish bone could be a potential source of a near-pure aragonite that could be mined directly to isolate it for fine uses.

**SEM microscopic** images show that after deproteinization, the chitin surface (Fig.8a) reveals a network composed of ordered and well-defined nanofibrils. In contrast, after deacetylation, the chitosan surface shows a network of fibrils that lose direction, non-ordered and amorphous (Fig.8b). According to these observations and the XRD results, it appears that deacetylation leads to the destruction of the crystalline structure, and to the decrease of the number of intermolecular hydrogen bonds generating a more or less amorphous structure confirmed by the previously calculated. SEM of the internal structure of cuttlefish bone from a 3D cut block (Fig.8c), showed a microstructure characterized by regular layered sheets, with lamellar spacing that facilitates buoyancy to the animal.

The degree of deacetylation (DDA) of chitosan was determined by potentiometry according to the equation described by *Tolaimate et al.*, [10, 33]. The titration curves obtained each present two inflection points (Fig.9). The difference between these two points corresponds to the amount of acid consumed for the neutralization of the amine groups. The DDA of chitosan calculated, is 91.89%. The $^{1}$H-NMR spectra (400 MHz, DCl, 70°C) of β-chitin and its derivative chitosan respectively extracted from cuttlefish bone are shown in Figure 10. In Figure 10a, the chitin spectra show the characteristic resonances of the acetylated α anomer and β anomer at 5.4 and 4.9 ppm, respectively. The resonant α and β anomer proton at 3.02 and 3.28 ppm, respectively, interfere with H-2 of the N-deacetylated units. The acetyl protons resonate at 2 ppm, with an intense peak as a result of the high acetyl number in chitin, while the other ring protons resonate in the range between 3.6 and 4 ppm. Acid hydrolysis (DCl 20%) of glycosidic bond (β 1-4), eliminated the appearance of the reducing end resonances of the α and β anomer from a deacetylated unit, which are expected to appear at 5.65 and 5.21 ppm [48, 49]. $^{1}$H-NMR

is considered is the best and most accurate method currently available to accurately calculate the DDA [50], [51], [52]. The integrals of the H-1-D peak and the integral of the H-Acetyl peak, are used to calculate the DDA of chitosan according to the following formula [53]:

$$\textbf{DDA (\%)} = \frac{(\mathbf{H-1-D})}{(\mathbf{H-1-D + 1/3\ HAc})} \times \mathbf{100}$$

With H-1-D is the integration of the H1 proton of glucosamine (H1-D, integrated at 1) and H-Acetyl (CH3) is the integration attributed to the proton peak assigned to the acetyl group (H-Acetyl, integrated at 0.16). The DDA determined a by NMR is 96.15%, this is in agreement with potentiometry. This verifies that the N-deacetylation reaction according to the Brussignac process was successfully performed with a molecular weight of 94.712 g/mol (95 KDa) and a measured viscosity of 472 ml/g according to the equation previously described by Mark Houwink [32].

The thermogram (TGA/DSC) of aragonite (Fig.11a), reveals a mass loss in three stages which are related to three endothermic transitions. The first two losses in the ranges 300-350°C and 410-460°C correspond to the release of carbon dioxide resulting from the combustion of the organic fraction. These two mass losses are thus relative to the loss of the organic matrix. The last loss is important located in the range between 670 and 895°C. The maximum degradation temperatures ($DTG_{max}$) for aragonite is 839°C. It is due to the release of carbon dioxide following the transformation of bicarbonate into calcite oxide (CaO) at high temperatures. These results are in the same direction as the previous works [54]. The thermograms of chitin (Fig.11b) and chitosan (Fig.11c) reveal a mass loss in two steps that are related to two endothermic transitions. The first mass loss can be attributed to the evaporation of water molecules at temperatures between 100°-250°C for both macromolecules. The second loss is endothermic and significant located in the range of 320° and 580°C, which can be attributed to the degradation or decomposition of the polysaccharide backbone and polymerization and/or decomposition of the acetylated and deacetylated units. In addition, $DTG_{max}$ for chitin and chitosan are approximately 328°C and 314°C respectively. This difference in $DTG_{max}$, could be due to the decrease in thermal stability which indicates the formation of chitosan [55].

### 3.3. Biocomposite characterization

The CHS/ArgS biocomposite, produced by freeze-drying, exhibits a sponge-like structure (Fig.12). The spectrum of the CHS/ArgS hybrid scaffold reveals the presence of characteristic bands associated with both chitosan and aragonite functional groups (Fig.13). In comparison with the CHS spectrum, the CHS/ArgS spectrum exhibits aragonite-specific bands, such as the phosphate groups at 580.88 $cm^{-1}$ and 1075.92 $cm^{-1}$, as well as the carbonyl function at 714 $cm^{-1}$ and the carbonate ion at 851 and 1496 $cm^{-1}$ [56]. Furthermore, compared with ArgS, the CHS/ArgS spectrum shows two peaks corresponding to amine groups I and II at 1647.91 $cm^{-1}$ and 1327.30 $cm^{-1}$, highlighting the presence of chitosan in the scaffold structure. XRD of CHS shows two characteristic peaks, a peak at 10° (2θ) the scaffold shows a peak at 20° (2θ), XRD of ArgS shows a halo between 15° and 35° (2θ). These two CHS peaks disappeared in the CHS/ArgS composite, confirming its interaction with the ArgS polymorph. Introducing the amorphous aspect of chitosan into the composite decreased the intensities of aragonite, especially the three reflections of the (012), (111) and (221) planes relative to aragonite which is coherent with other results (Fig.14) [56]. SEM micrographs of the aragonite surface and the CHS/ArgS biocomposite show that aragonite microparticles are introduced into the chitosan structure (Fig.15).

### 4.4. In-vitro bioactivity assays:

#### 4.4.1. XRD analysis of apatite layer

XRD structural analysis of the bioactive apatite layer is employed to elucidate the precipitation process of mineral apatite on the aragonite and biocomposite surface after immersion in SBF solution, according to soaking kinetics of 3 days, 7 days, 15 days and 30 days. The formation of hydroxyapatite serves as a control for the bioactivity of aragonite and biocomposite. Immersion of aragonite alone in SBF reveals characteristic hydroxyapatite peaks only from 15 days of immersion, with the emergence of a peak at 26°θ corresponding to the (211) plane (Fig.16a). By contrast, immersion of the biocomposite shows the same peak from day three. After 30 days of immersion, the XRD diagram of the biocomposite shows four peaks at 26°θ, 31°θ, 32°θ and 33°θ, corresponding respectively to the (002), (211), (112) and (300) plane reflections of the hydroxyapatite crystals (Fig.16b). In addition, the hydroxyapatite peaks formed on the biocomposite surface are sharper than those of aragonite, highlighting better crystallization of the apatite layer on the biocomposite. The results obtained underline that the transformation of aragonite into a hydroxyapatite layer requires a considerable amount of time, whereas the introduction of chitosan into the CHS/ArgS biocomposite significantly accelerates

the rapid appearance of the apatite layer on the biocomposite surface. The presence of chitosan promotes interactions and ionic exchanges between the biocomposite and its environment, while positively influencing the crystallization quality of the apatite layer formed. Similar work has been carried out on bioactivity [25].

#### 4.4.2. FTIR analysis of apatite layer

FTIR spectra of aragonite and biocomposite after 3 days, 7 days, 15 days and 30 days soaking in SBF solution are shown in Figure 17a and 17b. To assess the interactions and bonds formed in the prepared biomaterials, the IR spectrum of synthetic hydroxyapatite is used as a reference [57-58]. Following soaking in SBF solution, the structure of aragonite and biocomposite undergoes changes due to interfacial chemical reactions between these biomaterials and the physiological solution, leading to the formation of an apatite layer. The IR spectrum of the biocomposite reveals the appearance of three new, well-defined phosphate bands at 566.609 and 1035 $cm^{-1}$ after three days soaking in physiological solution. These bands are attributed to stretching vibrations of the $PO_4^{3-}$ group in the phosphate crystalline phases. Simultaneously, carbonate bands at 879 and 1443 $cm^{-1}$ are also observed, testifying to C-O bending vibration and C-O stretching vibration respectively in the carbonate groups. These results remain virtually the same for the 7-day, 15-day and 30-day timescales, confirming the formation of a bone-like carbonated hydroxyapatite layer on the biocomposite surface after soaking in SBF. On the other hand, after three days' immersion in the SBF solution, the aragonite spectrum does not show the characteristic bands of the apatite layer. Only after seven days' immersion do the phosphate and carbonate group bands appear. Moreover, the characteristic bands identified on the IR spectrum of the biocomposite are more clearly defined than those of the aragonite. This confirms the quality of apatite crystallization on the biocomposite surface. These results are in perfect agreement with XRD analyses, highlighting the positive impact of the chitosan polymer on the bioactivity of aragonite.

#### 4.4.3. Microstructure by SEM

The Figure 18 shows SEM micrographs of the aragonite and biocomposite surfaces after 3 days and 30 days soaking in SBF solution. Hydroxyapatite crystals begin to form on the biocomposite surface as early as day 3. In contrast, the aragonite surface shows no hydroxyapatite crystals within this timeframe. After 30 days of immersion, the biocomposite surface is completely coated with apatite crystals (Fig.18B’), all of similar shape. In contrast,

the aragonite surface begins to exhibit a developing hydroxyapatite layer, corroborating the results obtained by XRD. These results confirm the rapid formation of a dense apatite layer on the biocomposite surface, this layer being more visible than that overlying the aragonite. This facilitates the transport of $Ca^{2+}$ and $PO_4^{3-}$ ions from the physiological fluid onto the biocomposite surface. These results are in line with numerous studies on the bioactivity of glass and chitosan [58-59]. Furthermore, the observations confirm the quality of crystallization of the apatite layer on the surface of the CHS/ArgS biocomposite. The association of chitosan with aragonite shows positive effects in improving the formation and crystallization of the hydroxyapatite layer.

#### 4.4.4. ICP-OES analysis

The variation of calcium and phosphorus ion concentrations in the SBF solution as a function of immersion time reflects the exchanges between the material and SBF that are linked to the formation of the hydroxyapatite layer. The Ca/P phosphocalcium ratio is a valuable marker of the purity of the hydroxyapatite layer. For aragonite (Fig.16), the concentration of calcium ions in the SBF solution analyzed decreases from 100 ppm to 90 ppm after 3 days of immersion. This explains the release of calcium from aragonite into SBF. The calcium ion concentration remains virtually constant until day 7$^e$, then decreases very gradually until day 30 of immersion, highlighting the slow effect of calcium ion deposition on the aragonite surface in preparation for apatite formation. For the CHS/ArgS biocomposite (Fig.16), the calcium ion concentration increases slowly after 3 days of immersion, from 100 ppm to 106 ppm. This increase is consistent with the release of available calcium from the aragonite during the dealkalization process. After day 3, this concentration falls rapidly until the last day of immersion (30 days). This decrease corresponds to the precipitation of calcium ions on the biocomposite surface to form the apatite layer. This could be attributed to the presence of chitosan, which promotes the dissolution of calcium ions. This effect is similar to the behavior of bioactive glass with the chitosan molecule [25, 58-59]. Figure 17 shows the evolution of phosphorus ion concentrations in SBF as a function of immersion time. For ArgS, the phosphorus concentration decreases from 30 ppm to 20 ppm after 3 days of immersion, reflecting the transfer of phosphorus to the aragonite. Thereafter, phosphorus ion concentration gradually decreases until the last day of immersion, reaching 3 ppm, as phosphorus is mobilized in the formation of the calcium phosphate layer. For the CHS/ArgS biocomposite, the phosphorus ion concentration decreases significantly from 30 ppm to 13 ppm after 3 days of immersion. Compared with aragonite,

chitosan accelerates the utilization of phosphorus ions by the biocomposite, a phenomenon that can be attributed to the participation of these ions in the formation of the hydroxyapatite layer. Moreover, chitosan promotes dissolution three times faster than aragonite on days 7 and 15, resulting in faster phosphorus consumption by the biocomposite than by ArgS. These results concur with analyses obtained by XRD, FTIR and SEM.

# 4. Conclusion

In conclusion, this study demonstrates the viability of valorizing marine cuttlebone (*Sepia officinalis*) waste as a source of chitin-aragonite composite matrix. Analysis of this biowaste revealed a composition comprising 62% aragonite, 11% chitin and 27% minerals/proteins. The composition of the dorsal and ventral faces was studied by ICP-OES, showing a predominant Ca composition with 67.95 and 141.89 ppm respectively. The crystallinity index of chitin and chitosan determined by XRD was 64.77 and 39.14% respectively. The degree of deacetylation of chitosan, assessed by $^{1}$H-NMR and potentiometry, was 96.15% and 91.89% respectively. Thermal analysis revealed that aragonite, chitin and chitosan degraded with $DTG_{max}$ of 839°C, 328°C and 314°C respectively. The intrinsic viscosity and molar mass of chitosan are 472 ml/g and 94.712 g/mol respectively, with better solubility in acetic acid (0.3%). The development of the CHS/ArgS biocomposite from the chitinous-aragonite matrix of cuttlefish bone by lyophilization revealed a bioactivity confirmed by the formation of a carbonated hydroxyapatite layer on the surface of these biomaterials during in vitro tests in SBF. In particular, the presence of the chitosan polymer enhanced the bioactivity of aragonite. These results highlighted the potential of biocomposites derived from marine waste for future biomedical applications, such as bone tissue engineering. However, further studies on biodegradability, cytocompatibility and in vitro testing in the presence of cells are needed to fully exploit the potential of these biocomposites. These promising data call for further research to maximize their use in innovative medical applications.

**Declarations**

**Ethical Approval and Consent to participate**

Not applicable

**Consent for publication**

Not applicable

**Availability of data and materials**

Not applicable

**Declaration of competing interest**

The authors declare that they have no competing interests

**Funding**

This work received no funding.

**Author's contributions**

YAH, SEL and BL were the major contributor in writing the manuscript. HO and MR revised the manuscript. All authors read and approved the final manuscript.

**Acknowledgements**

The authors express their gratitude, and thank Mrs. Christine deponge, NMR engineer at the Institute of Chemical Sciences of Rennes (ISCR), for her immense helpful for the authors of this study.

**Authors' information**

Not applicable

## References

[1] M. Rinaudo, and S. Perez, From chitin to chitosan. In: Glycopedia.eu. http://www.glycopedia.eu/IMG/pdf/from_chitin_to_chitosan.pdf. (2019). Accessed 11 May 2023.

[2] K. Kurita, Controlled functionalization of the polysaccharide chitin. Progress in Polymer science, 26(2001), 1921-1971.

[3] A.G. Checa, J.H.E. Cartwright, I.S. Almazo, J.P. Andrade, F.R. Raya, The cuttlefish Sepia officinalis (Sepiidae, Cephalopoda) constructs cuttlebone from a liquid-crystal precursor, Sci. Rep. 5 (2015), 11513–11526.

[4] E. Tkalčec, J. Popović, S. Orlić, S. Milardović, H. Ivanković, Hydrothermal synthesis and thermal evolution of carbonate-fluorhydroxyapatite scaffold from cuttlefish bones, Mater. Sci. Eng. C 42 (2014), 578–586.

[5] M. Florek, E. Fornal, P. Gómez-Romero, E. Zieba, W. Paszkowicz, J. Lekki, ..., A. Kuczumow, Complementary microstructural and chemical analyses of Sepia officinalis endoskeleton. Materials Science and Engineering: C, 29(2009), 1220-1226.

[6] F. Arrouze, J. Desbrieres, S. Lidrissi Hassani, A. Tolaimate, Investigation of β-chitin extracted from cuttlefish: comparison with squid β-chitin. Polymer Bulletin, 78(2021), 7219-7239.

[7] F. Arrouze, J. Desbrieres, M. Rhazi, M. Essahli, , A. Tolaimate, Valorization of chitins extracted from North Morocco shrimps: Comparison of chitin reactivity and characteristics. Journal of Applied Polymer Science, 136(2019), 47804.

[8] V. F. Lee, Univ Microflm. (1974) no. 74/29446.

[9] P. E. Austin, J. E. Castle, C. J. Albisetti, Appl Sci. Elsevier, Amsterdam. (1989), p 749

[10] A. Tolaimate, J. Desbrieres, M. Rhazi, and A. Alagui, Contribution to the preparation of chitins and chitosans with controlled physico-chemical properties. Polymer, 44 (2003), 7939-7952.

[11] M. M. Brzeski, Chitin and Chitosan putting waste to good use. (1987). Info fsh Int 5:31–33.

[12] A. Bhatnagar, M. Sillanpää, Applications of chitin- and chitosan-derivatives for the detoxifcation of water and wastewater—A short review. (2009). Adv Colloid Interface Sci 152(1–2):26–38.

[13] Y. Ait Hamdan, F. El Amerany, J. Desbrières, A. Aghrinane, H. Oudadesse, M. Rhazi, The evolution of the global COVID-19 epidemic in Morocco and understanding the different therapeutic approaches of chitosan in the control of the pandemic. Polymer Bulletin, 80(2022), 10633-10659.

[14] M. Rinaudo, Chitin and chitosan: properties and applications. Prog Polym Sci. (2006). 31(7):603–632.

[15] P. Morganti G. Morganti, Chitin nanofbrils for advanced cosmeceuticals. Clin Dermatol. (2008) 26(4):334–340.

[16] A. Bhatnagar, M. Sillanpää, "Applications of chitin- and chitosan-derivatives for the detoxifcation of water and wastewater"—A short review. Adv Colloid Interface Sci. (2009) 152(1–2):26–38.

[17] R. L. Smith, Brev. Américain, p 4 (1984), 474-769

[18] P. Sahariah, M. Másson, Antimicrobial chitosan and chitosan derivatives: a review of the structure–activity relationship. Biomacromolecules, 18(2017), 3846-3868

[19] H. Yi, L. Q. Wu, W. E. Bentley, R. Ghodssi, G. W. Rubloff, J. N. Culver, and G. F. Payne, Biofabrication with chitosan. Biomacromolecules, 6 (2005), 2881-2894.

[20] S. Van Vlierberghe, P. Dubruel, E. Schacht, Biopolymer-based hydrogels as scaffolds for tissue engineering applications: a review. Biomacromolecules, 12 (2011), 1387-1408.

[21] H. Wang, J. Qian, F. Ding, Emerging chitosan-based films for food packaging applications. Journal of agricultural and food chemistry 66.2 (2018): 395-413.

[22] M. Shahid, F. Mohammad, Green Chemistry Approaches to Develop Antimicrobial Textiles Based on Sustainable Biopolymers. A Review. Industrial & Engineering Chemistry Research, 52 (2013), 5245-5260.

[23] V. K. Thakur, M. K. Thakur, Recent advances in graft copolymerization and applications of chitosan: a review. ACS Sustainable Chemistry & Engineering, 2 (2014), 2637-2652.

[24] E. M. Gerhard, W., Li. C. Wang, Guo, J., Ozbolat, I. T., Rahn, K. M., ..., J. Yang, Design strategies and applications of nacre-based biomaterials. Acta biomaterialia, 54 (2017), 21-34.

[25] E. Toufik, H. Noukrati, C. Rey, O. Marsan, C. Charvillat, S. Cazalbou, ..., C. Combes, On the physicochemical properties, setting chemical reaction, and in vitro bioactivity of aragonite–chitosan composite cement as a bone substitute. New Journal of Chemistry, 47(6), (2023), 2771-2786.

[26] Y. A. Hamdan, S. Elouali, N. Eladlani, B. Lefeuvre, H. Oudadesse, M. Rhazi, Investigation on Akis granulifera (Coleoptera, Sahlberg, 1823) as a potential source of chitin and chitosan: Extraction, characterization and hydrogel formation. International Journal of Biological Macromolecules, 252 (2023), 126292.

[27] P. Broussignac, High natural polymer known in the industry: chitosan. Chim Ind Genie Chim 99 (1968), 1241–1247.

[28] J. Bumgardner, B. Chesnutt, W. Haggard, Y. Yuan, T. Utturkar, B. Reves, Patent Application No. 11/740, (2007),042.

[29] E. J. Lee, D. S. Shin, H. E. Kim, H. W. Kim, Y. H. Koh, J. H. Jang, Membrane of hybrid chitosan–silica xerogel for guided bone regeneration. Biomaterials, 30(5) : (2009) 743-750.

[30] F. Zhao, Y. Yin, W. W. Lu, J. C. Leong, W. Zhang, J. Zhang,..., K. Yao, Preparation and histological evaluation of biomimetic three-dimensional hydroxyapatite/chitosan-gelatin network composite scaffolds. Biomaterials, 23(15) : (2002) 3227-3234.

[31] T. Kokubo, H. Kushitani, S. Sakka, T. Kitsugi, T. Yamamuro, Solutions able to reproduce in vivo surface-structure changes in bioactive glass-ceramic A-W3. Journal of biomedical materials research, 24(6) : (1990) 721-734.

[32] T. Kokubo, H. Takadama, How useful is SBF in predicting in vivo bone bioactivity?. Biomaterials, 27(15) : (2006) 2907-2915.

[33] G. A. Roberts, Structure of chitin and chitosan. Chitin chemistry, (1992), 1-53.

[34] R.H. Chen, M.L. Tsaih, Effect of température on the intrinsic viscosity and conformation of chitosans in dulte HCl solution, international journal of biological. Macromolecules 23 (1998), 135-141.

[35] S. Liu, J. Sun, L. Yu, C. Zhang, J. Bi, F.Zhu, ..., Q. Yang, Extraction and characterization of chitin from the beetle Holotrichia parallela Motschulsky." Molecules 17.4 (2012), 4604-4611.

[36] L. Segal, J. Creely, AE. Martin, CM. Conrad, An empirical method for estimating the degree of crystallinity of native cellulose using the x-ray difractometer. Text Res J 29 (1959), 786–794.

[37] S. Hajji, I. Younes, O. Ghorbel-Bellaaj, R. Hajji, M. Rinaudo, M. Nasri, K. Jellouli. Structural diferences between chitin and chitosan extracted from three diferent marine sources. Int J Biol Macromol 65 (2014), 298–306.

[38] H. S. Jung, M. H. Kim, W. H. Park, Preparation and structural investigation of novel β-chitin nanocrystals from cuttlefish bone. ACS Biomaterials Science & Engineering, 5(4) (2019), 1744-1752.

[39] B. Focher, PL. Beltrame, A. Naggi, G. Torri, Alkaline N-deacetylation of chitin enhanced by fash treatments. Reaction kinetics and structure modifcations. Carbohydr Polym. 12(4) (1990), 405–418.

[40] B. Focher, A. Naggi, G. Torri, A. Cosani, M. Terbojevich, Structural diferences between chitin polymorphs and their precipitates from solutions-evidence from CP-MAS 13C-NMR FT-IR and FTRaman spectroscopy. Carbohydr Polym. 17(2) (1992), 97–102.

[41] H. S. Jung, M. H. Kim, J. Y. Shin, S. R. Park, J. Y. Jung, W. H. Park, Electrospinning and wound healing activity of β-chitin extracted from cuttlefish bone. Carbohydrate polymers, 193 (2018), 205-211.

[42] N. Nouj, N. Hafid, N. El Alem, I. I. Buciscanu, S. S. Maier, P. Samoila, ..., C. D. Stan, Valorization of β-Chitin Extraction Byproduct from Cuttlefish Bone and Its Application in Food Wastewater Treatment. Materials, 15(8) (2022), 2803.

[43] H. S. Jung, M. H. Kim, W. H. Park, Preparation and structural investigation of novel β-chitin nanocrystals from cuttlefish bone. ACS Biomaterials Science & Engineering, 5(4) (2019), 1744-1752.

[44] D. S Silva, J. AM Delezuk, F. A La Porta, E. Longo, S. P Campana-Filho, Comparison of experimental and theoretical data on the structural and electronic characterization of chitin and chitosan. Current Physical Chemistry, 5(3) (2015), 206-213.

[45] M. Florek, E. Fornal, P. Gómez-Romero, E. Zieba, W. Paszkowicz, J. Lekki, J. Nowak, A. Kuczumow. Complementary microstructural and chemical analyses of Sepia officinalis endoskeleton. Mater. Sci. Eng. C 29 (2009), 1220–1226.

[46] J. Kumirska, M. Czerwicka, Z. Kaczyński, A. Bychowska, K. Brzozowski, J. Thöming, and P. Stepnowski, Application of spectroscopic methods for structural analysis of chitin and chitosan. Marine drugs, 8 (2010), 1567-1636.

[47] A. S. Darwish, D. I. Osman, H. A. Mohammed, S. K. Attia, Cuttlefish bone biowaste for production of holey aragonitic sheets and mesoporous mayenite-embedded Ag2CO3 nanocomposite: Towards design high-performance adsorbents and visible-light photocatalyst for detoxification of dyes

[48] A. Einbu, K. M. Varum, Depolymerization and de-N-acetylation of chitin oligomers in hydrochloric acid. Biomacromolecules. 8(2007), 309–314.

[49] K. M. Vårum, M. H. Ottøy, O. Smidsrød, Carbohydr. Polym. 46 (1) (2001), 89–98.

[50] R. Czechowska-Biskup, D. Jarosińska, B. Rokita, P. Ulański, J. M. Rosiak, Determination of degree of deacetylation of chitosan-comparision of methods. Progress on Chemistry and Application of Chitin and its Derivatives, 17(2012),5-20.

[51] Y. Zhang, X. Zhang, R. Ding, J. Zhang, J. Liu, Determination of the degree of deacetylation of chitosan by potentiometric titration preceded by enzymatic pretreatment. Carbohydrate Polymers, 83(2011), 813-817.

[52] Y. Rohyami, N. A. Sari, Simple method on determination of deacetyllation degree for chitosan. In AIP Conference Proceedings (Vol. 2370, No. 1, p. 030003), (2021), AIP Publishing LLC.

[53] M. Lavertu, Z. Xia, A. N. Serreqi, M. Berrada, A. Rodrigues, D. Wang, A. Gupta, A validated 1H-NMR method for the determination of the degree of deacetylation of chitosan. Journal of pharmaceutical and biomedical analysis, 32(2003), 1149-1158.

[54] J. Venkatesan, P. D. Rekha, S. Anil, I. Bhatnagar, P. N. Sudha, C. Dechsakulwatana, ..., M. S. Shim, Hydroxyapatite from cuttlefish bone: isolation, characterizations, and applications. Biotechnology and Bioprocess Engineering, 23 (2018), 383-393.

[55] M. Kaya, M. Asan-Ozusaglam, S. Erdogan, Comparison of antimicrobial activities of newly obtained low molecular weight scorpion chitosan and medium molecular weight commercial chitosan. Journal of bioscience and bioengineering, 121(6) (2016), 678-684.

[56] I. Ghosh, C. Sharma, R.Tandon, Structural evaluation of chitosan-modified precipitated calcium carbonate composite fillers for papermaking applications. SN Applied Sciences, 2, (2020)1-14.

[57] P. Luo, Methods of synthesizing hydroxyapatite powders and bulk materials (No. US 5858318). Lawrence Livermore National Lab.(LLNL), Livermore, CA (United States) (1999).

[58] X. V. Bui, H. Oudadesse, Y. Le Gal, O. Merdrignac-Conanec, G. Cathelineau, Bioactivity behaviour of biodegradable material comprising bioactive glass. Korean Journal of Chemical Engineering, 29 (2012), 215-220.

[59] X. V. Bui, H. Oudadesse, Y. Le Gal, A. Mostafa, G. Cathelineau, Microspheres of chitosan-bioactive glass for application in orthopedic surgery. In vitro experiment. Recent Researches in Modern Medicine, (2011) 359-367.

**Graphical Abstract :**

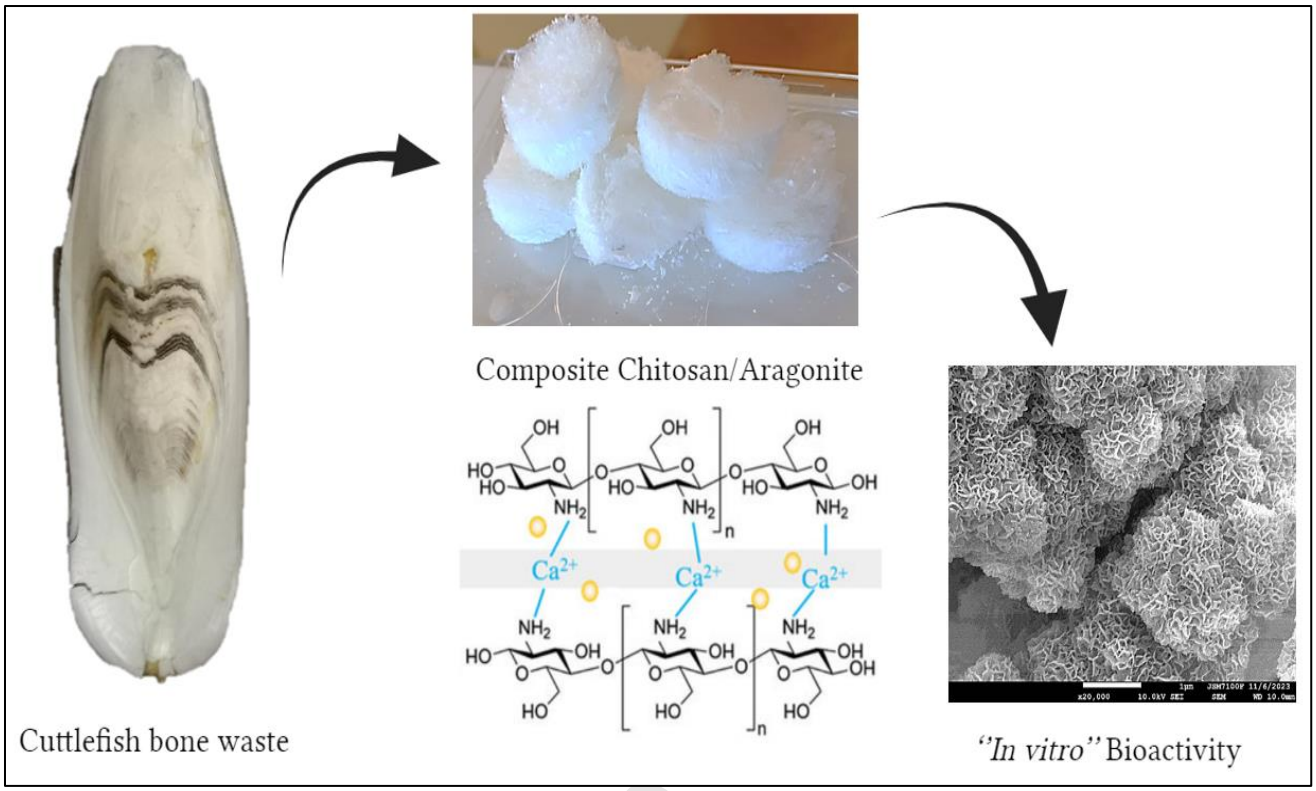




## Figures

**Figure 1:** Ventral and dorsal views of the cuttlebone

**Figure 2:** Schematic composition (a) and steps of chitin extraction and chitosan preparation from cuttlefish (b).

**Figure 3:** FT-IR spectra of aragonite (a), chitin (b), and chitosan (c) from cuttlefish.

**Figure 4:** XRD of the organo-inorganic complex of cuttlefish bone.

**Figure 5:** XRD of chitin and chitosan visualized after separation from complex.

**Figure 6:** XRD of aragonite ($CaCO_3$) after isolation on the ventral side of cuttlefish bone.

**Figure 7:** XRD model of comparison of aragonite with synthetic reference aragonite and calcite.

**Figure 8:** SEM images of the dorsal surface illustrate the fibrillar organization of organic constituents, including chitin (a), giving rise to chitosan after deacetylation (b), while the ventral side illustrates the organized structure of aragonite in the form of cross-sectional chambers (c).

**Figure 9:** Titration curve to determine the degree of deacetylation of chitosan.

**Figure 10**: $^{1}$H-NMR spectrum (400 MHz, DCl/D2O, 70°C) of chitin (a) chitosan (b).

**Figure 11:** TGA/DSC of aragonite (a), chitin (b) and chitosan (c) from cuttlefish.

**Figure 12:** Chitosan/aragonite composite sponges obtained by freeze-drying.

**Figure 13:** FT-IR spectra of biocomposite chitosan/aragonite (CHS/ArgS), chitosan (CHS) and aragonite (ArgS).

**Figure 14:** XRD of biocomposite chitosan/aragonite (CHS/ArgS), chitosan (CHS) and aragonite (ArgS).

**Figure 15:** SEM images of CHS (a), ArgS (b) and biocomposite CHS/ArgS (c) (scale bars 500 µm ; x 10,000)

**Figure 16:** XRD of ArgS (a) and CHS/ArgS biocomposite (b) after 3, 7, 15 and 30 days of soaking in SBF solution and Hydroxyapatite.

**Figure 17:** FT-IR spectra of ArgS (a) and CHS/ArgS biocomposite (b) after 3, 7, 15 and 30 days of soaking in SBF solution and Hydroxyapatite.

**Figure 18:** SEM images of ArgS (A,A') and CHS/ArgS biocomposite (B,B') after 3 and 30 days soaking in SBF solution (scale bars 500 µm; x 10,000).

**Figure 19:** Evolution of elemental concentrations of Ca in SBF solution measured by ICP-OES, versus soaking times.

**Figure 20:** Evolution of elemental concentrations of P in SBF solution measured by ICP-OES, versus soaking times.

**Fig. 1**


**Fig. 2**

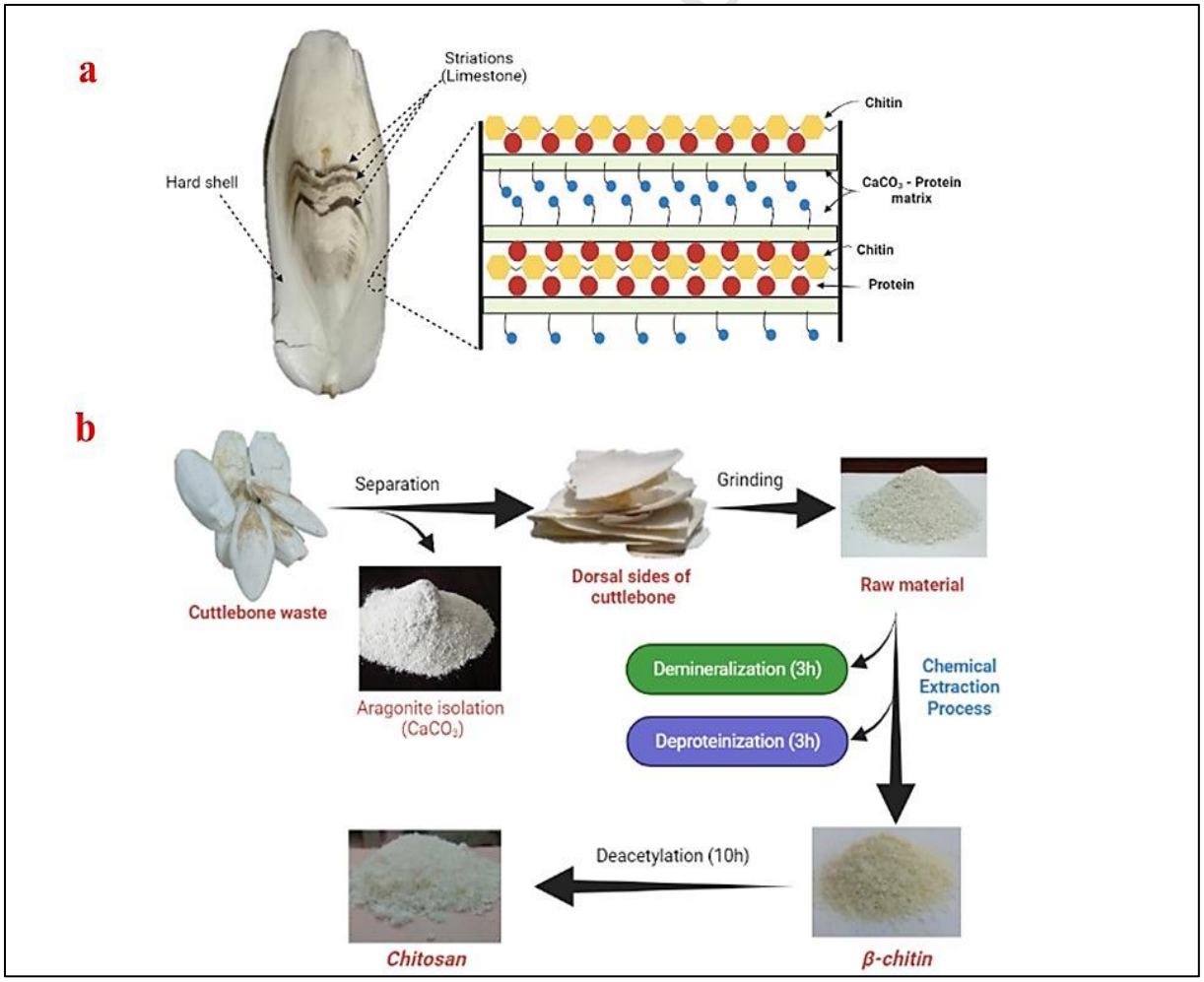

**Fig. 3**

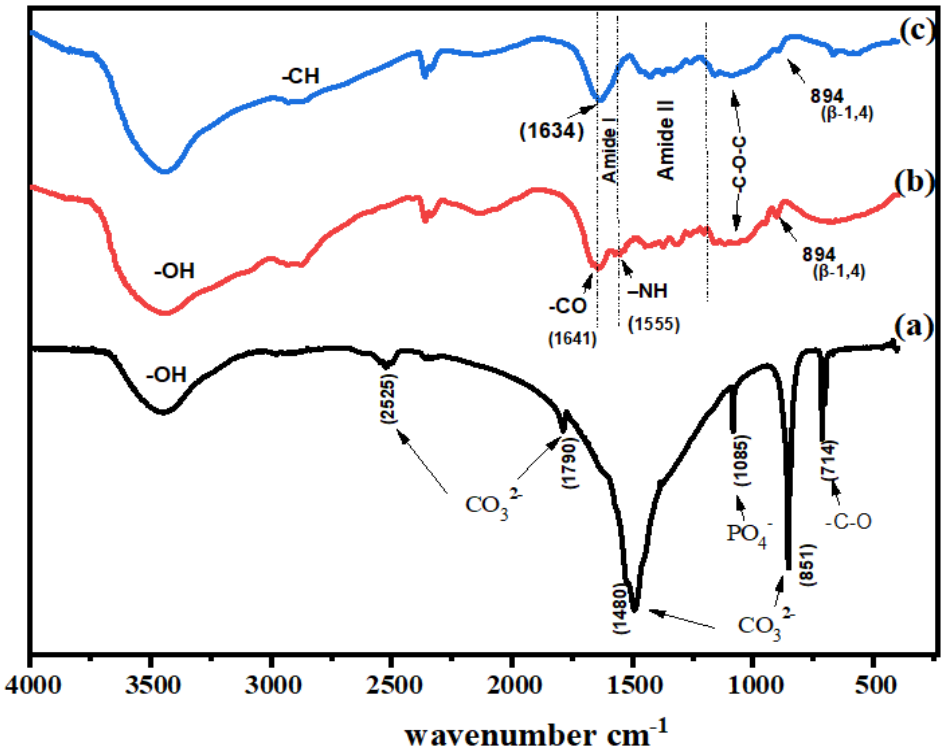
(c)
-CH
(1634)
Amide I
Amide II
-C-O-C
894
(β-1,4)
(b)
-OH
-CO
(1641)
-NH
(1555)
894
(β-1,4)
(a)
-OH
(2525)
(1790)
$CO_3^{2-}$
(1085)
$PO_4^-$
(714)
-C-O
(851)
(1480)
$CO_3^{2-}$
4000
3500
3000
2500
2000
1500
1000
500
wavenumber $cm^{-1}$

**Fig. 4**

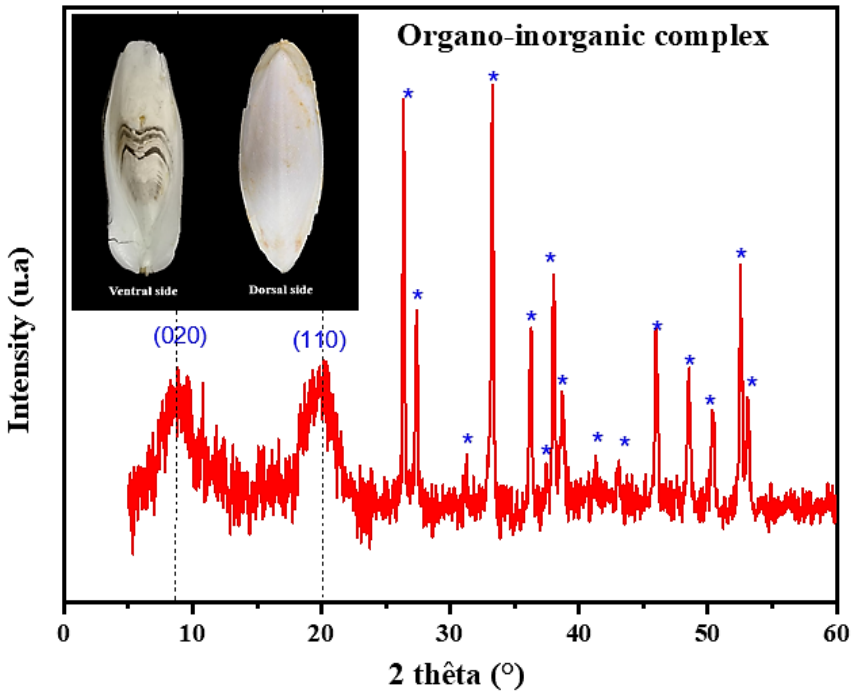
Organo-inorganic complex
Ventral side
Dorsal side
(020)
(110)
Intensity (u.a)
0
10
20
30
40
50
60
2 thêta (°)

Fig. 5

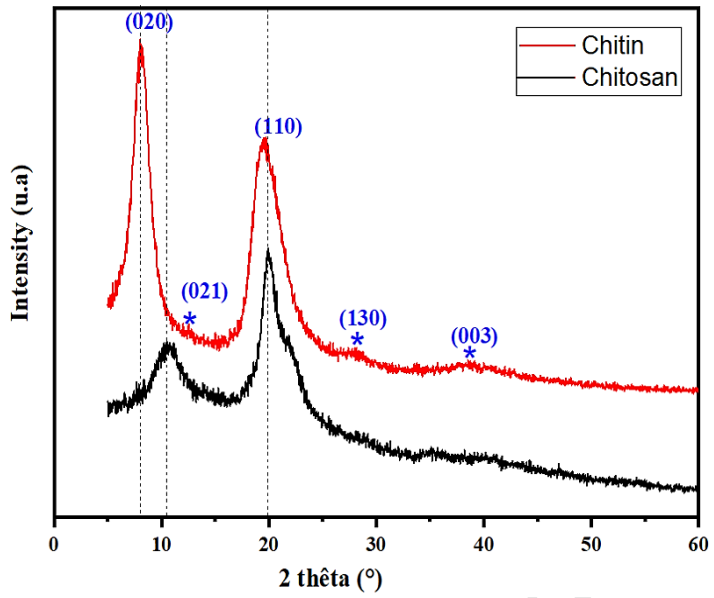


Fig. 6

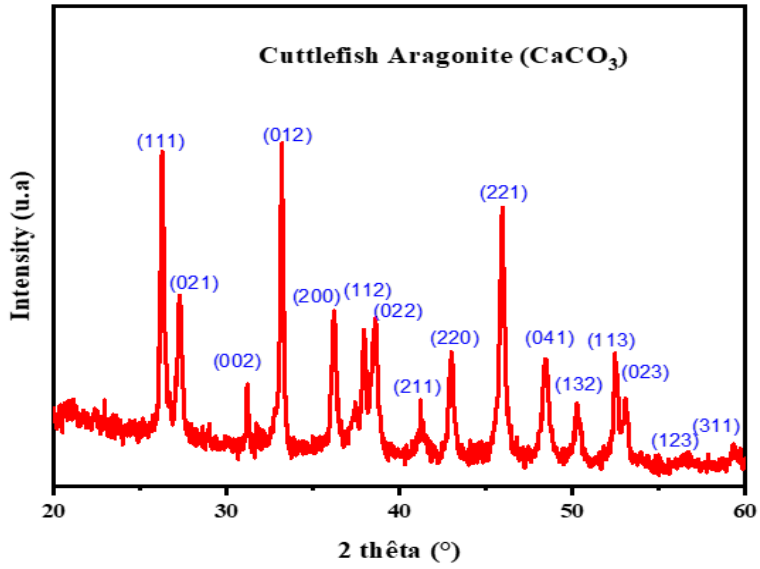


Fig. 7

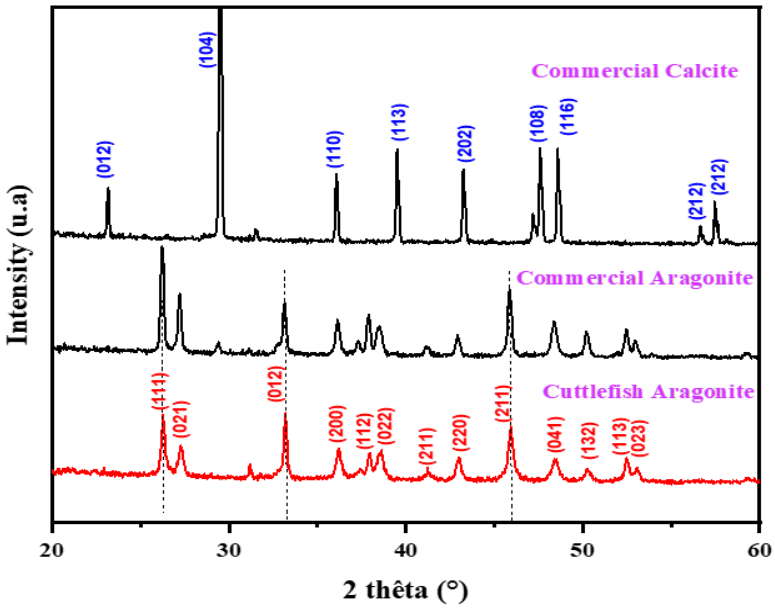

Fig. 8

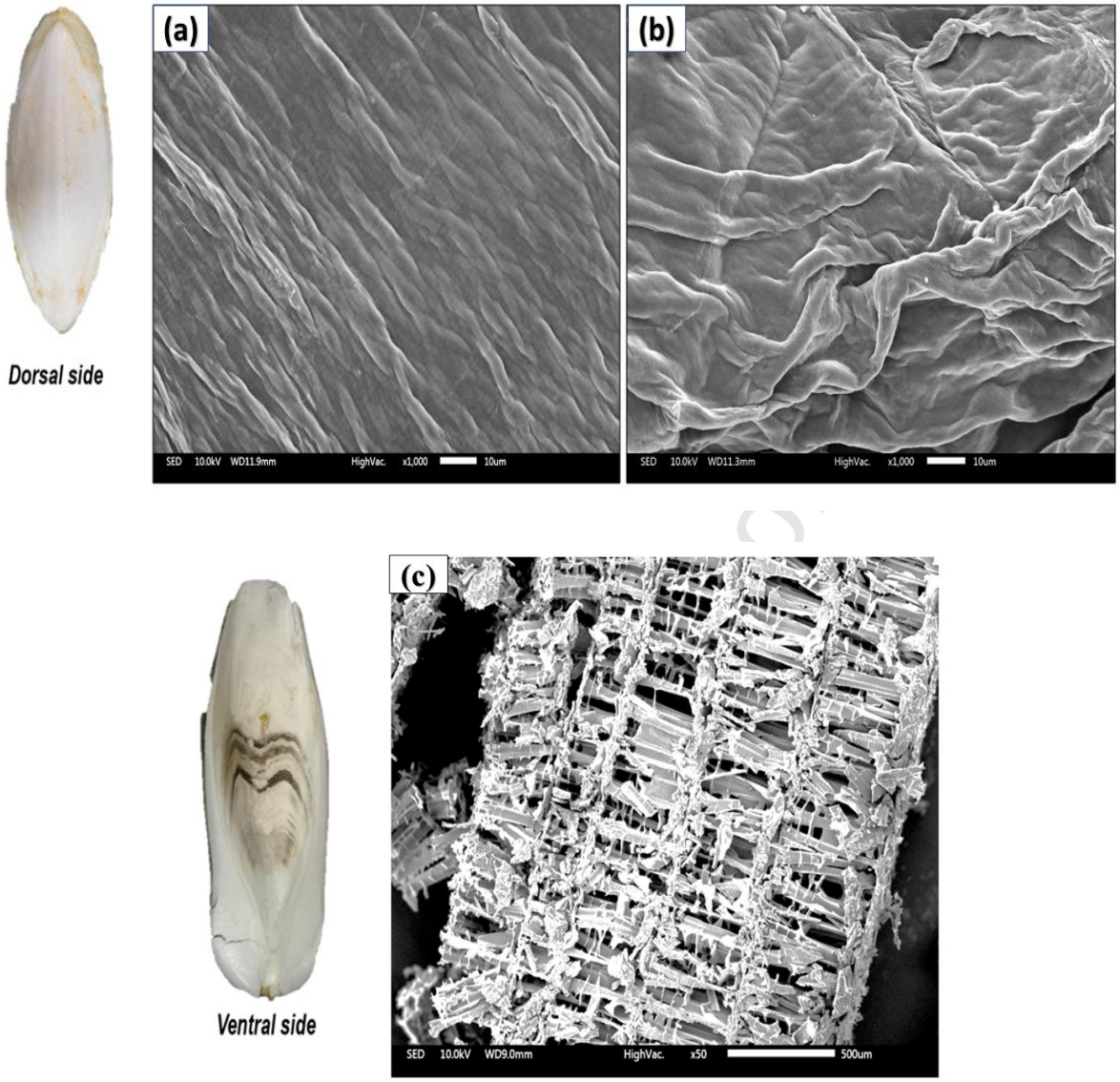
Dorsal side
(a)
(b)
SED 10.0kV WD11.9mm HighVac. x1,000 10um
SED 10.0kV WD11.3mm HighVac. x1,000 10um
Ventral side
(c)
SED 10.0kV WD9.0mm HighVac. x50 500um

Fig. 9

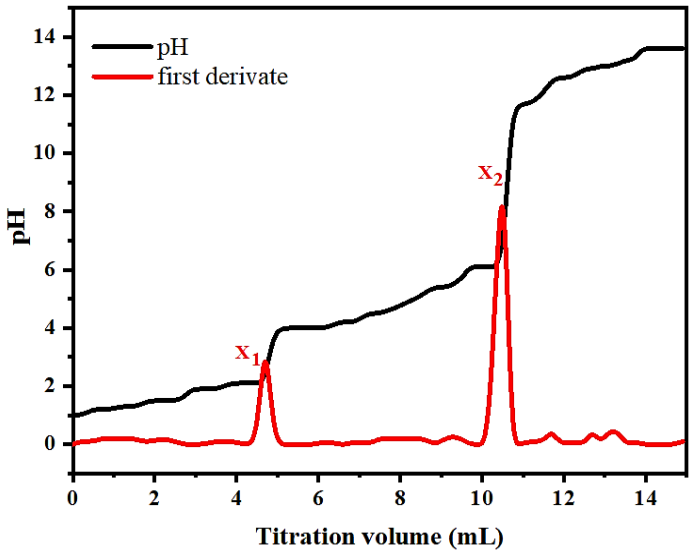
pH
first derivate
x1
x2
pH
Titration volume (mL)
0
2
4
6
8
10
12
14

**Fig. 10**

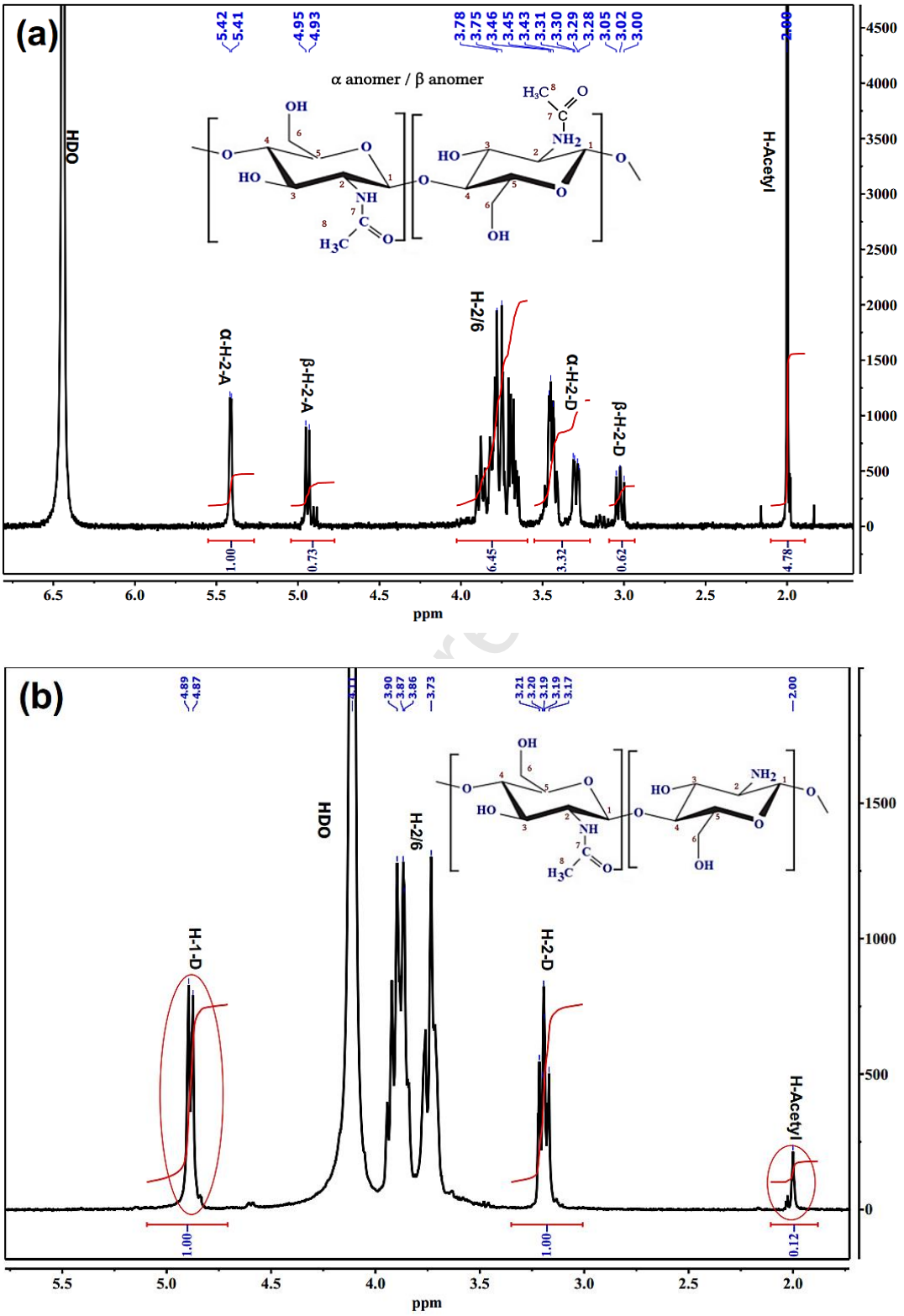
(a)
HDO
α anomer / β anomer
H-Acetyl
α-H-2-A
β-H-2-A
H-2/6
α-H-2-D
β-H-2-D
1.00
0.73
6.45
3.32
0.62
4.78
ppm
(b)
HDO
H-2/6
H-1-D
H-2-D
H-Acetyl
1.00
1.00
0.12
ppm

**Fig. 11**

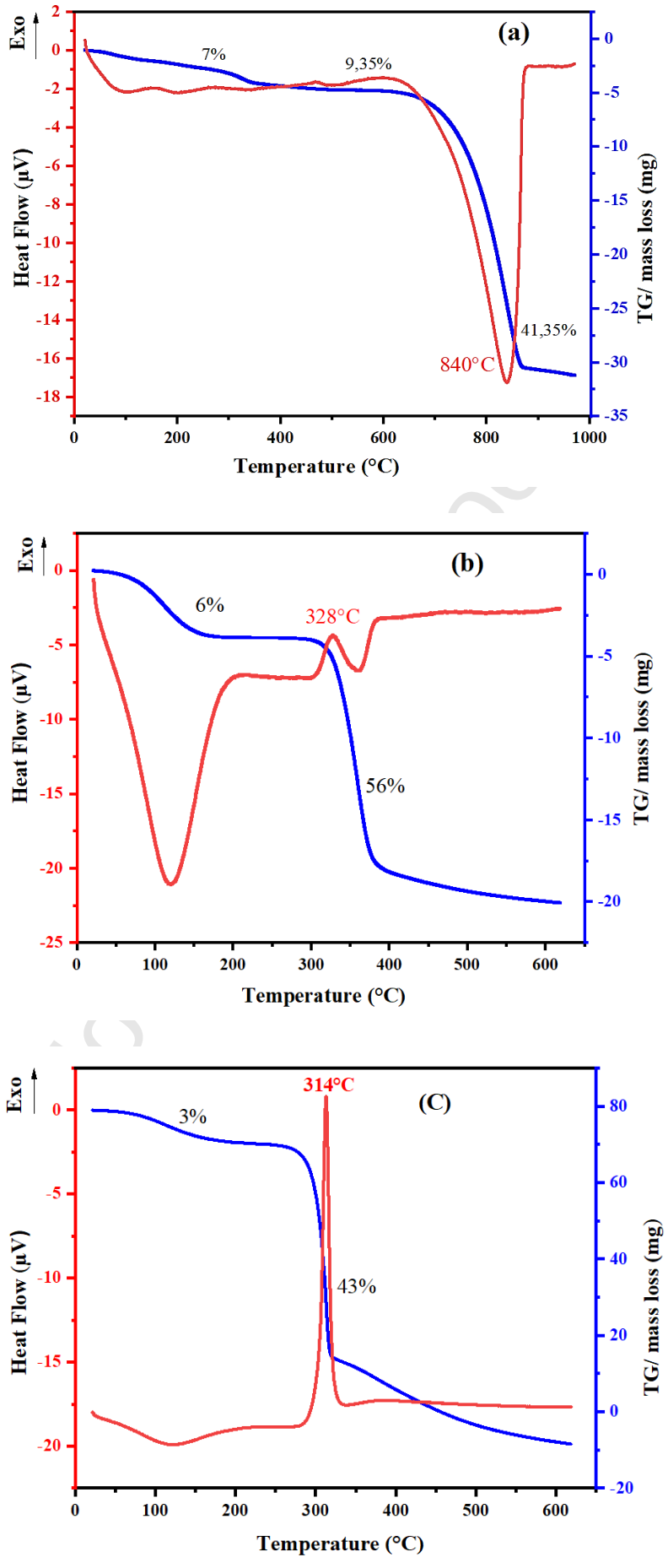
(a)
Exo
Heat Flow (µV)
TG/ mass loss (mg)
Temperature (°C)
7%
9,35%
41,35%
840°C
(b)
6%
328°C
56%
(C)
314°C
3%
43%

**Fig. 12**

**Fig. 13**

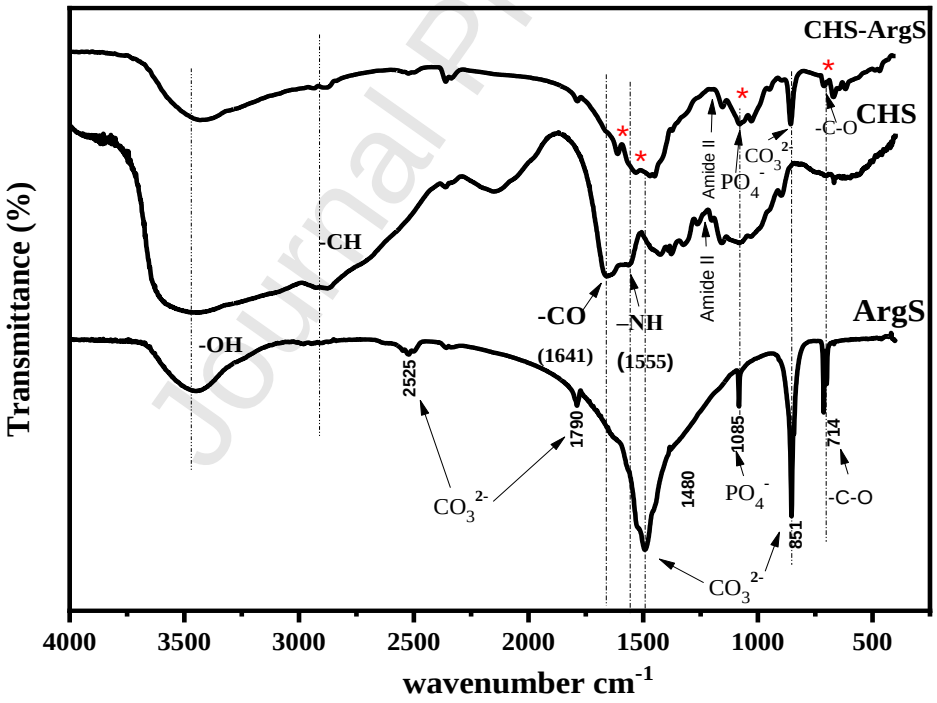

**Fig. 14**

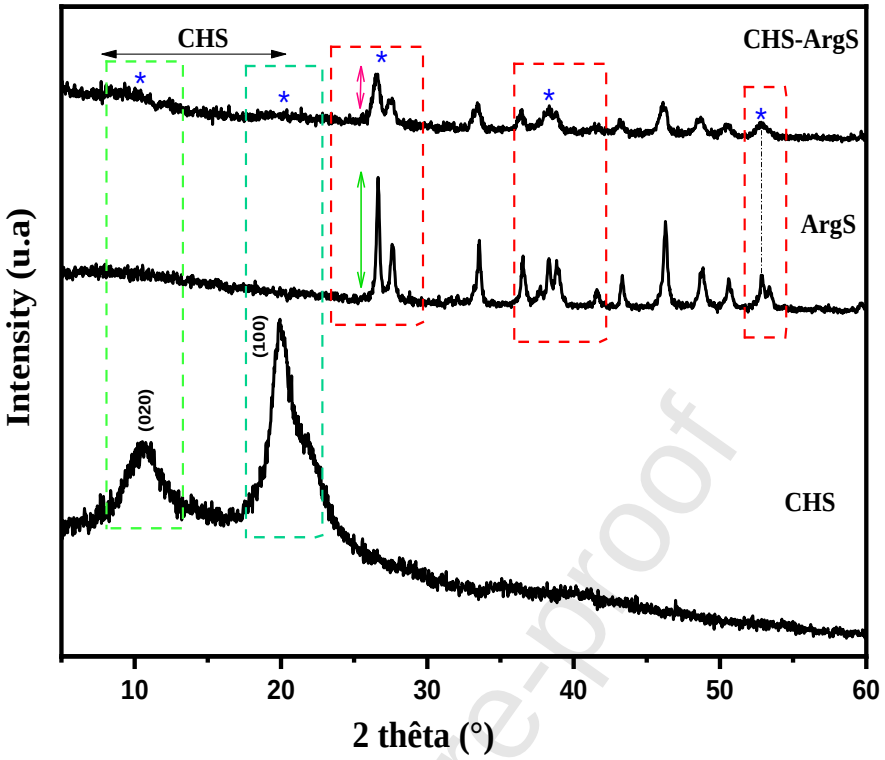
CHS
CHS-ArgS
ArgS
CHS
(020)
(100)
*
Intensity (u.a)
10
20
30
40
50
60
2 thêta (°)

**Fig. 15**

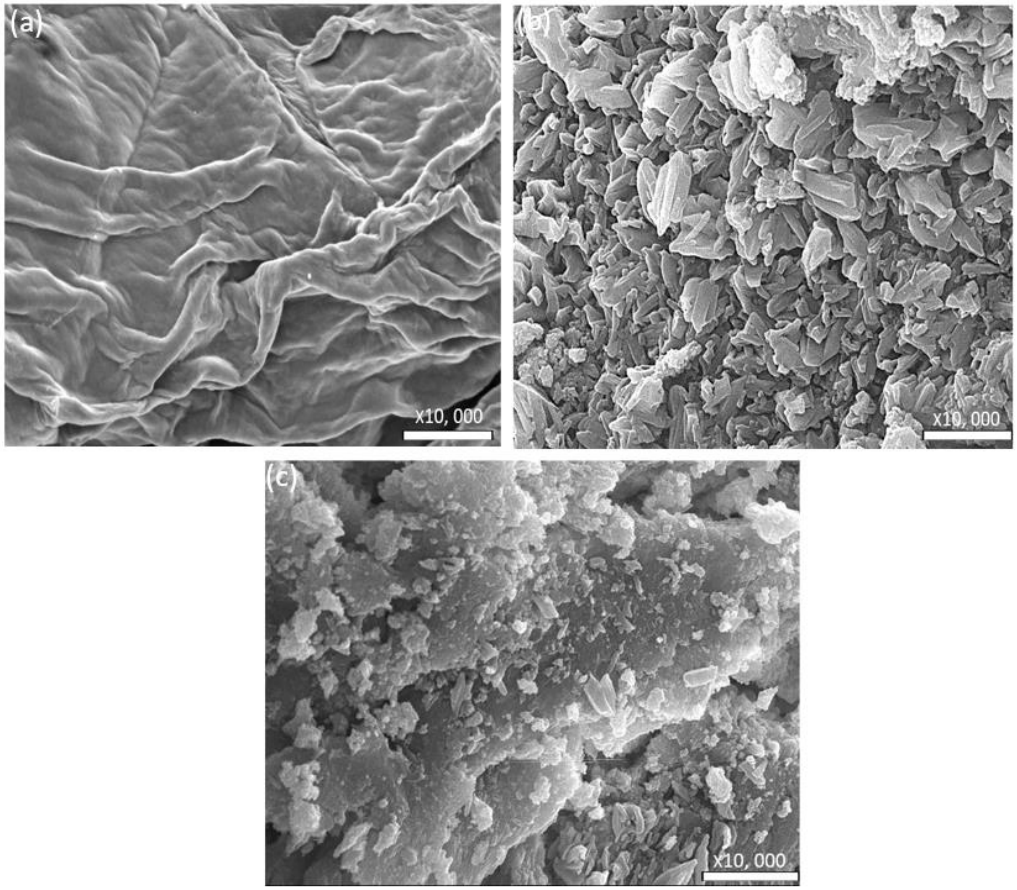
(a)
x10, 000
(b)
x10, 000
(c)
x10, 000

**Fig. 16**

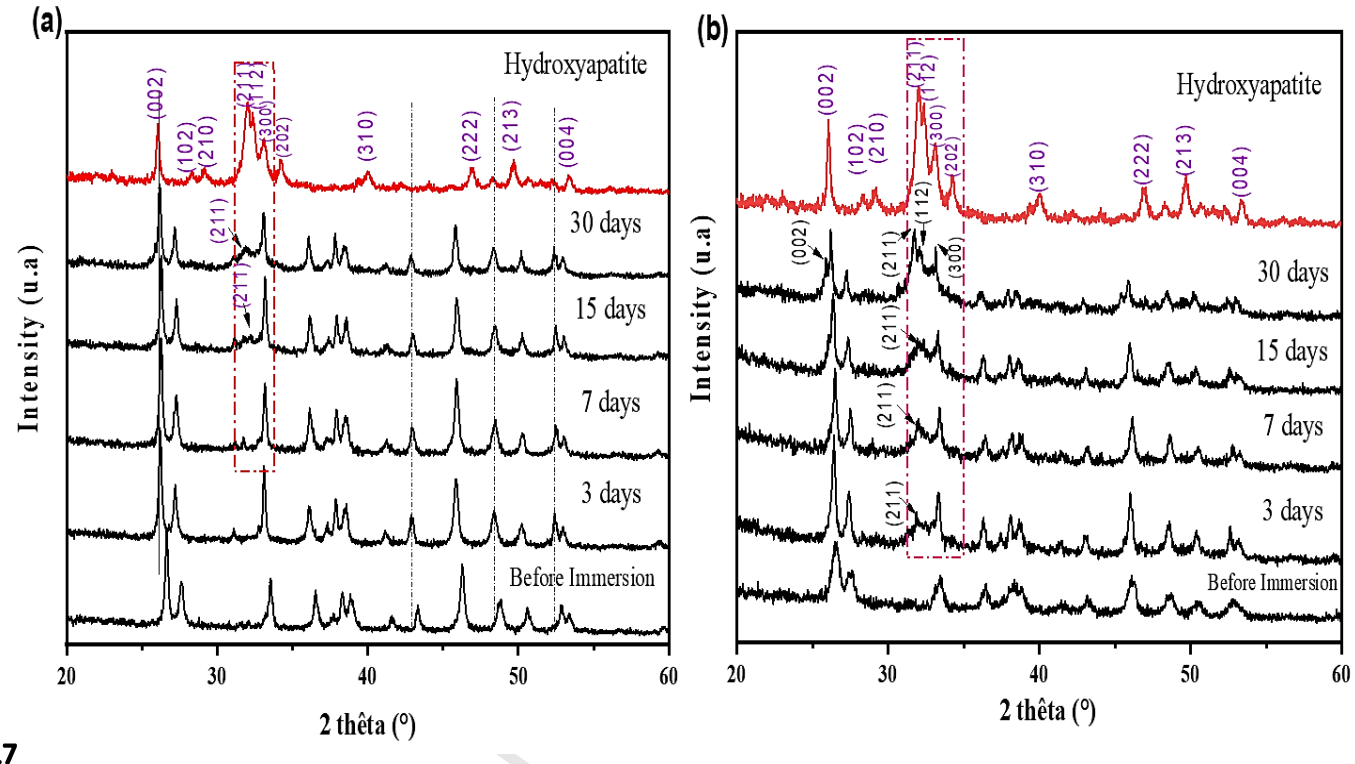
(a)
(b)
Hydroxyapatite
30 days
15 days
7 days
3 days
Before Immersion
(002)
(102)
(210)
(211)
(112)
(300)
(202)
(310)
(222)
(213)
(004)
Intensity (u.a)
2 thêta (°)

**Fig. 17**

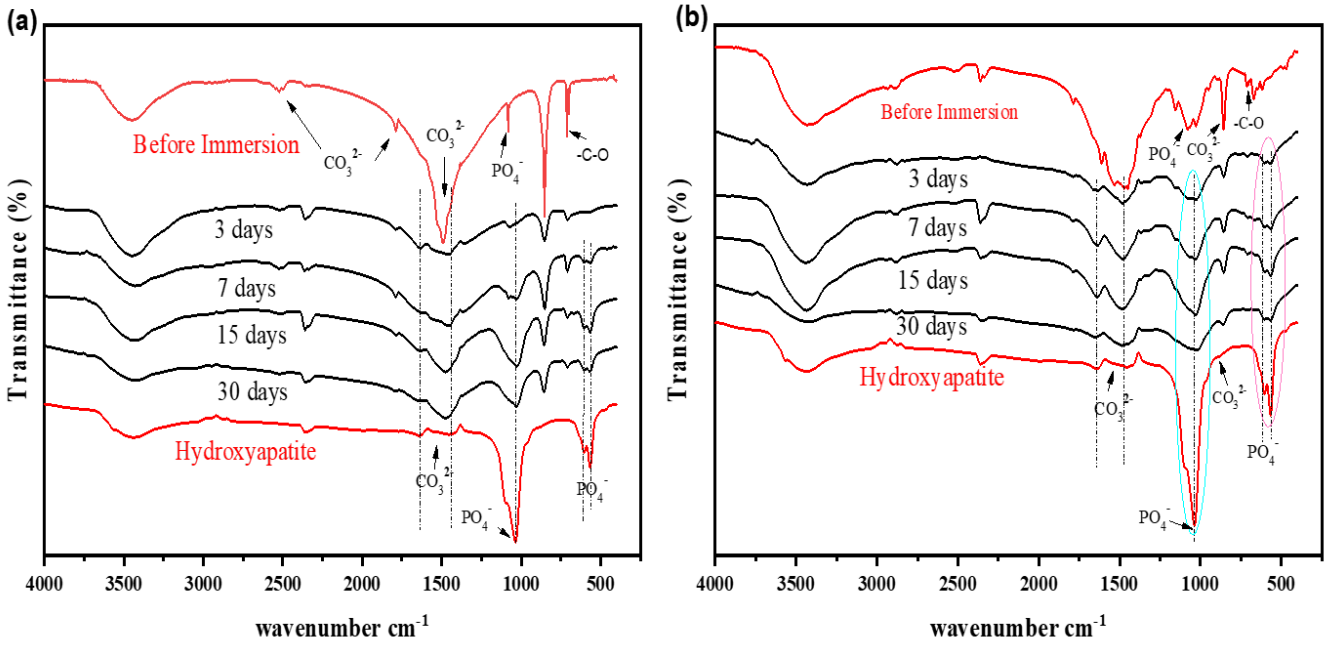
(a)
(b)
Before Immersion
3 days
7 days
15 days
30 days
Hydroxyapatite
$CO_3^{2-}$
$PO_4^-$
-C-O
Transmittance (%)
wavenumber $cm^{-1}$

Fig. 18

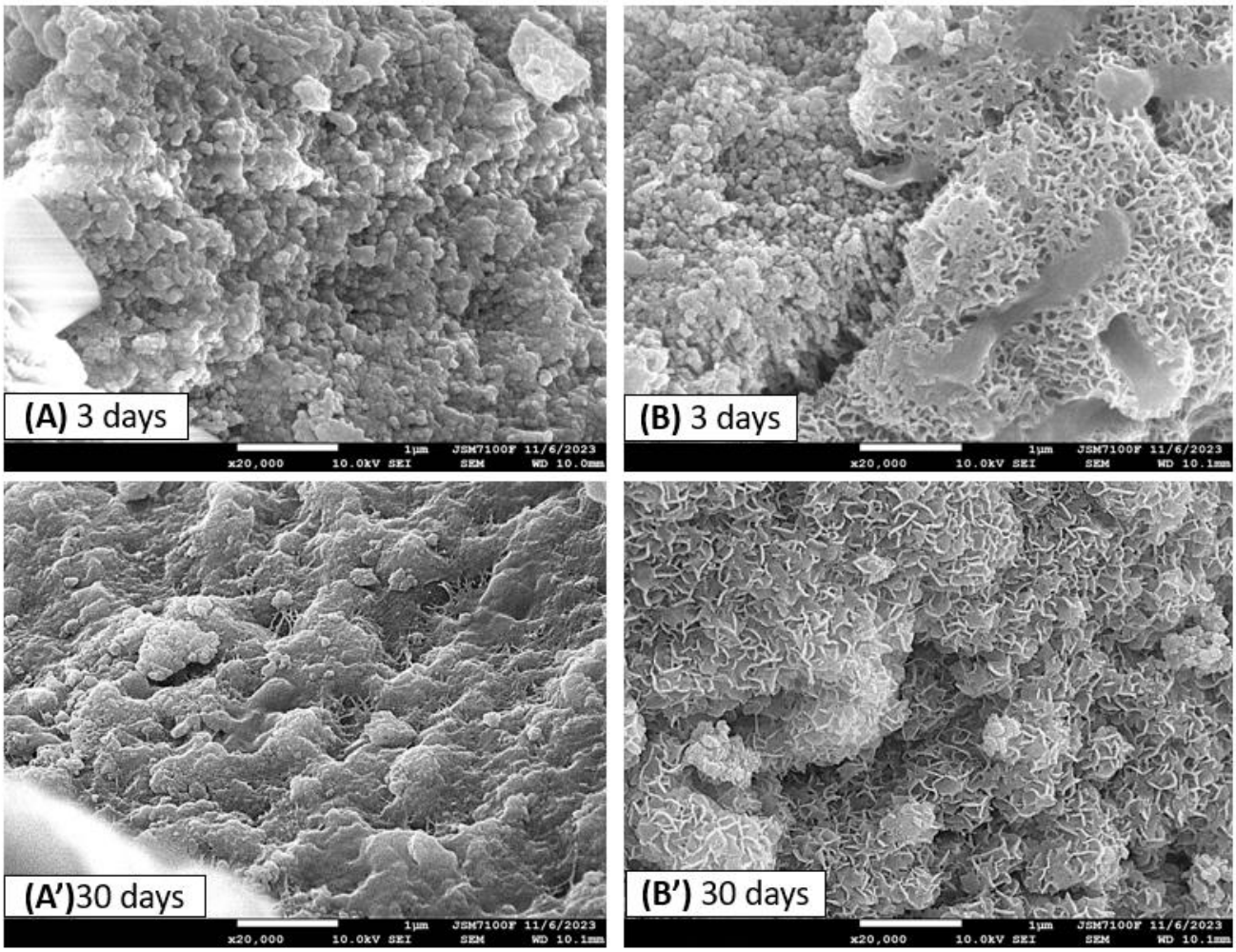
(A) 3 days
(B) 3 days
(A')30 days
(B') 30 days

Fig. 19

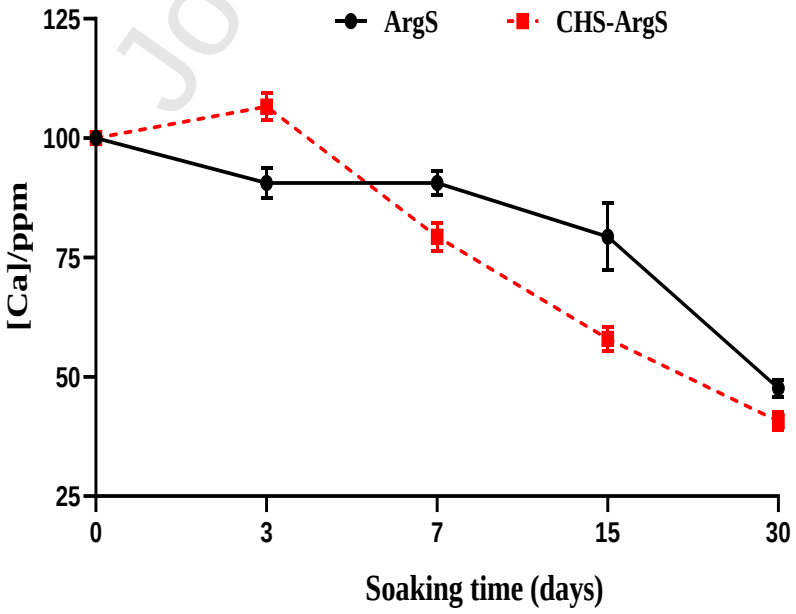
ArgS
CHS-ArgS
[Ca]/ppm
125
100
75
50
25
0
3
7
15
30
Soaking time (days)

Fig. 20

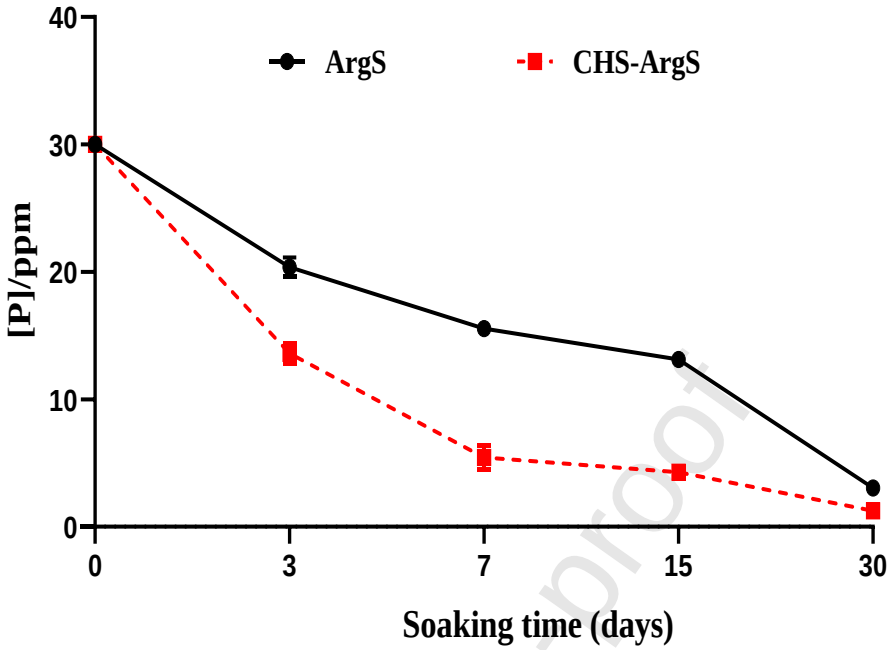


## Tables

**Table 1.** Concentrations of the SBF solution.

| | Ionic concentrations $10^{-3}$ mol.L$^{-1}$ | | | | | | |
|---|---|---|---|---|---|---|---|
| | $Na^+$ | $K^+$ | $Ca^{2+}$ | $Mg^{2+}$ | $Cl^-$ | $HCO_3^-$ | $HPO_4^{2-}$ |
| **SBF** | 142 | 5 | 2.5 | 1.5 | 148.8 | 4.2 | 1 |
| **Plasma** | 142 | 5 | 2.6 | 1.6 | 103.0 | 27.0 | 1 |

**Table 2.** Chemical composition of the dorsal and ventral side of the cuttlebone

| | Ca | Na | Sr | P | Al | Si | Zn |
|---|---|---|---|---|---|---|---|
| **Dorsal side (mg/l)** | 67.9 ± 1.2 | 0.78 ± 0.09 | 0.10 ± 0.05 | 0.29 ± 0.08 | 0.12 ± 0.01 | 0.11 ± 0.01 | 0.54 ± 0.03 |
| **Ventral side (mg/l)** | 141.8 ± 3.6 | 7.14 ± 0.71 | 1.04 ± 0.31 | 0.67± 0.09 | 0.11 ± 0.07 | 0.29 ± 0.02 | 0.00 ± 0.00 |

**Table 3.** FT-IR data of chitin and chitosan from cuttlefish bone

| Functional group | Chitin | Chitosan |
|---|---|---|

**Tableau 4.** XRD parameters of chitin and chitosan from cuttlefish bone

| | | | |
|---|---|---|---|
| ***OH stretching*** | ***3400-3560 cm-1*** | ***3260-3450 cm-1*** |
| ***NH stretching*** | ***3250-3260 cm-1*** | ***3250–3310 cm-1*** |
| ***CH2 vibration*** | ***2938-2869 cm-1*** | ***2938-2869 cm-1*** |
| ***C=O*** | ***1641 cm-1*** | ***1634 cm-1*** |
| ***NH (bending)*** | ***1555 cm-1*** | ***1540 cm-1*** |

| | *2θ(°)* | *d(Å)* | *Ir (%)* | *Icr (%)* |
|---|---|---|---|---|
| **Chitin** | **8.17** | **9.07** | **83.37** | |
| | **12.44** | **4.56** | **20.19** | |
| | **19.50** | **6.87** | **100.00** | **64.77** |
| | **27.82** | **4.63** | **12.06** | |
| | **38.72** | **3.28** | **19.62** | |
| **Chitosan** | **10.42** | **8.29** | **40.37** | **39.14** |
| | **20.03** | **4.47** | **100.00** | |

## Abstract:

Cuttlefish bone biowaste is a potential source of a composite matrix based on chitin and aragonite. In the present work, we propose for the first time the elaboration of biocomposites based on chitosan and aragonite through the valorization of bone waste. The composition of the ventral and dorsal surfaces of bone is well studied by ICP-OES. An extraction process has been applied to the dorsal surface to extract β-chitin and chitosan with controlled physico-chemical characteristics. In parallel, aragonite isolation was carried out on the ventral side. The freeze-drying metrhod was used to incorporate aragonite into the chitosan polymer to form CHS/ArgS biocomposites. Physicochemical characterizations were performed by FT-IR, SEM, XRD, $^{1}$H-NMR, TGA/DSC, potentiometry and viscometry. The ICP-OES method was used to evaluate in vitro the bioactivity level of biocomposite in simulated human plasma (SBF), enabling analysis of the interactions between the material and SBF. The results obtained indicate that the CHS/ArgS biocomposite derived from cuttlefish bone exhibits bioactivity, and that chitosan enhances the bioactivity of aragonite. The CHS/ArgS biocomposite showed excellent ability to form an apatite layer on its surface. After three days' immersion, FTIR and SEM analyses confirmed the formation of this layer.


**Key words**: Cuttlefish bone waste, Aragonite, Chitin, Chitosan, Physicochemical properties, biocomposite, biactivity